JACS
JOURNAL OF THE AMERICAN CHEMICAL SOCIETY

Article

pubs.acs.org/JACS

Theoretical Study of the Molecular Ordering, Paracrystallinity, And Charge Mobilities of Oligomers in Different Crystalline Phases

Ilhan Yavuz, Blanton N. Martin, Jiyong Park, and K. N. Houk*

Department of Chemistry and Biochemistry, University of California, Los Angeles, California 90095, United States

Supporting Information

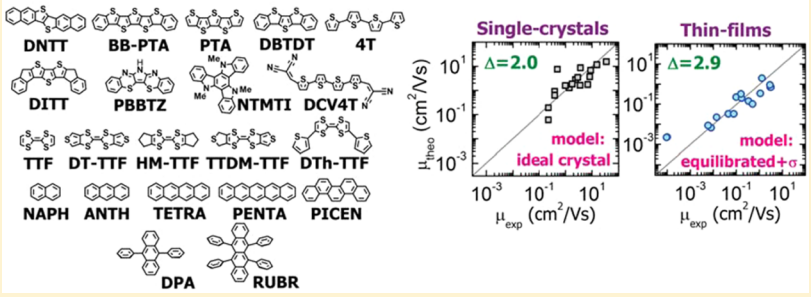

ABSTRACT: Molecular ordering and charge transport have been studied computationally for 22 conjugated oligomers fabricated as crystal or thin-film semiconductors. Molecular dynamics (MD) simulations are employed to equilibrate crystal morphologies at 300 K. The paracrystalline order parameter, *g*, is calculated to characterize structural order in the materials. Charge-transport dynamics are predicted using kinetic Monte Carlo methods based on a charge-hopping mechanism described by the Marcus theory of electron transfer to calculate charge-transfer rates using the VOTCA package. We introduce an error function to assess the reliability of our computed values to reproduce experimental hole mobilities in both crystalline and thin-film morphologies of the 22 conjugated oligomers. For each of the oligomers, we compute hole mobility with three different theoretical models incorporating increasing measures of disorder: (1) a perfect crystal, based on the experimentally derived crystal structure, with no disorder, (2) an MD-equilibrated structure incorporating thermal disorder into the crystal structure, and (3) model 2 above but also incorporating energetic disorder arising from variations in site energies. For the series of known crystals with long-range order, we find that the perfect crystal model produces hole mobilities giving the best fit to experimental data. For the series of thin-film morphologies with short-range order, we observe that the presence of both thermal and energetic disorder is essential for accurate calculation. We also discuss the interplay between hole mobility and other charge-transport parameters in these morphologies, such as reorganization energy and energetic disorder.

INTRODUCTION

Organic electronics have attracted much attention as low-cost, diverse, processable, and tunable materials.[1−5] Rapid progress in organic material design and device engineering has led to significant improvement in devices like organic field-effect transistors (OFET),[4,6] organic light emitting diodes (OLED),[7,8] and organic solar cells (OSC).[5] The performance of organic semiconducting materials, commonly characterized by charge-carrier mobilities, is shown to be competitive with the performance of amorphous silicon-based inorganic semiconductors and approaching to that of polycrystalline silicon.[3] For example, crystal rubrene transistors with mobilities of up to 15 $cm^2/(V\ s)$ have been reported,[9,10] along with a variety of thin-film transistors with mobilities on the order of 1−5 $cm^2/(V\ s)$.[11−13] Theoretical progress has been slow due to limited understanding of the fundamental properties of organic materials at the atomistic level. However, promising methodologies have been proposed to understand structure and transport properties to link microscopic features to overall device characteristics.[14−19]

How molecular structure, packing arrangement, and inherent disorder in self-assembled crystals control charge transport is still unclear and a matter of some controversy.[17,20] Small oligomeric semiconducting materials are useful due to their straightforward morphologies.[21,22] The crystalline phases of oligomers and the resulting charge-transport properties are also well understood.[3,4] Due to their advantages of long-range structural order, low impurities, and lack of grain boundaries, single-crystalline materials generally yield higher mobilities than polycrystalline thin films.[4] Theoretical characterization of crystals is also appealing as a means of understanding intrinsic transport properties and to provide the first step toward elucidating more sophisticated crystalline phases.[15,23−26]

We have performed charge-transport simulations on a large number of π-conjugated oligomers using three different computational models which differ by the level of disorder introduced. The key quantity, hole mobility, is extracted from these multiscale simulations and compared with experimentally

Received: August 5, 2014
Published: February 6, 2015

DOI: 10.1021/ja5076376
J. Am. Chem. Soc. 2015, 137, 2856−2866

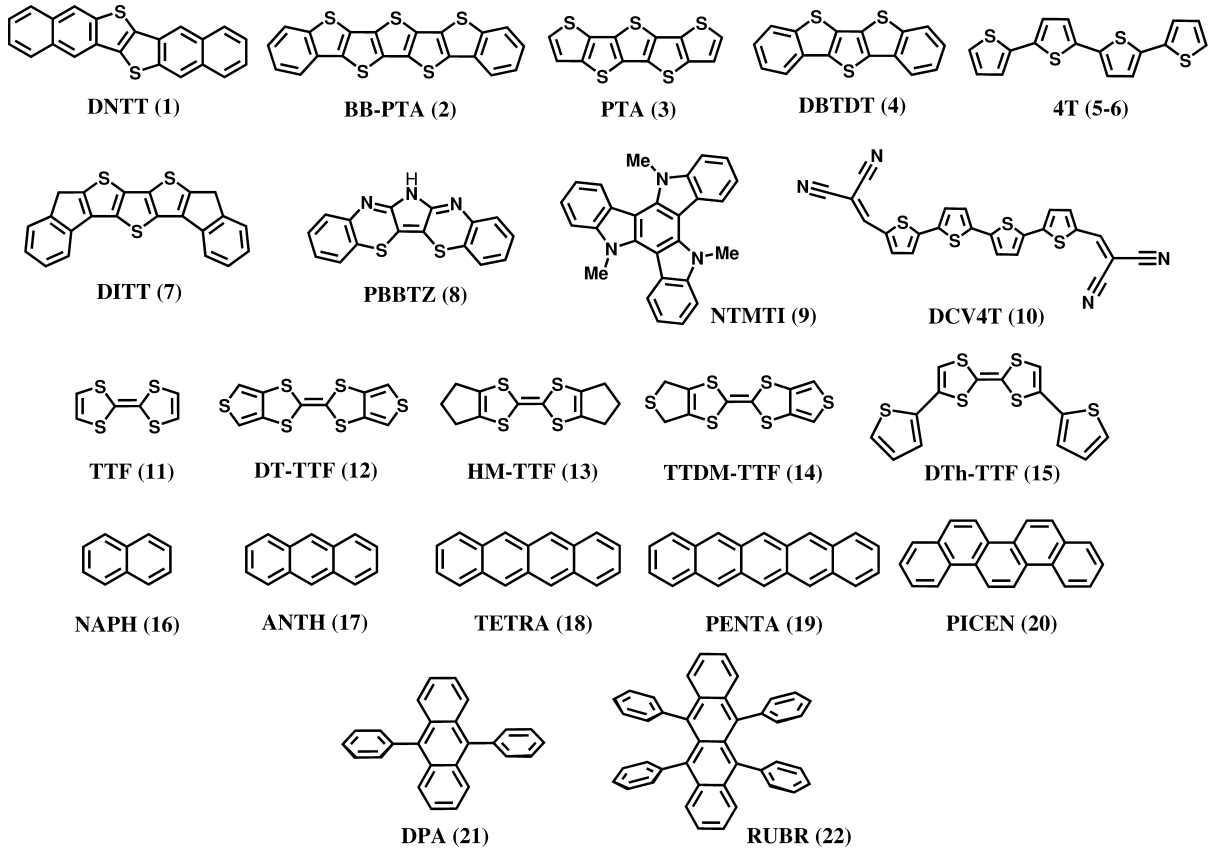

Figure 1. The 22 π-conjugated oligomers studied in this work. Full names of the oligomers are provided in Table S1. Note: two polymorphs of 4T (4T/HT and 4T/LT) are considered.

available crystal and/or thin-film mobility for each oligomer in order to gain insight into their morphological identities and resulting properties. The conjugated systems under study include oligoacenes, oligothiophenes, oligothienoacenes, tetrathiafulvalenes, and fused or functional derivatives of these systems, such as picene, *N*-trimethyltriindole, and pyrrolobisbenzothiazine (see Figure 1). These oligomeric systems are widely studied in the literature[3,4,27] and are often regarded as prototypes for advanced systems in organic electronic devices.[28−30] Because experimental crystal and thin-film hole mobilities have been measured for these oligomers, we can compare calculated mobilities from different theoretical models to the experimental data and investigate correlations between hole mobility and other charge-transport parameters, such as geometrical reorganization energies and energetic disorder.

Throughout the paper, we use the term 'packing motif' to refer to a molecular packing arrangement on the order of a unit cell whereas the term 'morphology' for larger scales, i.e., typically on the order of 10−20 nm.

MODELING MATERIAL MORPHOLOGY

For the charge-transport simulations of each oligomer, three different models were taken into account: (1) the disorder-free ideal crystal structure, (2) the crystal after incorporating thermal disorder, and (3) the crystal after incorporating both thermal and energetic disorder. In model 1, the ideal crystal configurations were constructed by successive duplications of the unit cells obtained from XRD measurements. Here, structural disorder arising from thermal and energetic disorder is neglected. In model (2), the system is brought to thermal equilibrium using atomistic molecular dynamics (MD) simulations to account for structural disorder arising from vibrations in the crystal, however energetic disorder is neglected. For model (3), energetic disorder is added to the equilibrated morphologies by a correction for the differences in site energies for each dimer pair in the simulation.

Charge-transport simulations in crystalline or disordered systems were performed using the VOTCA package.[31,32] The morphologies for charge-transport analysis are determined from ideal crystals (based on unit-cells) or from atomistic MD trajectories. After this, the hopping sites are determined to compute transport parameters (electronic coupling, reorganization energy, and site energies) and charge-carrier hopping rates.[33,34] Charge-transport dynamics are then performed, for a single charge carrier in a box with periodic-boundary conditions, using kinetic Monte Carlo algorithm.[32] Finally, hole mobility is calculated using velocity averaging.[35]

All MD simulations were performed using GPU accelerated version of Amber12.[36] Molecular mechanics parameters were prepared using the GAFF force field following a recommended procedure described elsewhere.[37,38]The supramolecular packing geometry was energy minimized in 1000 MD steps, where all heavy atom coordinates were restrained to their initial values. Each system was heated and equilibrated at 300 K for 4 ns while regulating heat bath temperature at 300 K using a Langevin thermostat[39] with a weak collision parameter (5.0 ps^{-1}). An additional 2 ns relaxation was carried out with a Berendsen barostat[39] to relax the system at 1 atm. The production run lasted for 20 ns while maintaining a heat bath temperature of 300 K and a time-averaged pressure of 1 atm.

DOI: 10.1021/ja5076376
J. Am. Chem. Soc. 2015, 137, 2856−2866

MOLECULAR STRUCTURE

The series of oligomer structures studied is shown in Figure 1. This series consists of oligomers with relatively planar rigid fragments or multiple rigid fragments bridged by rotatable single bonds. Oligomers labeled as **1**−**4**, **7**, and **16**−**20** consist of fused thiophene, benzene, and/or cyclopentene rings with no rotatable single bonds. **8** and **9** are also relatively rigid because they contain fused benzothiazine and pyrrole moieties, and **5**, **6**, **10**, and **21**−**22** contain multiple rigid fragments linked by rotatable single bonds. TTF and its derivatives **11**−**14** are distinct because they possess relatively planar fragments linked by a double bond. Finally, **15** consists of a TTF backbone with substituted thiophene rings.

CRYSTAL STRUCTURES AND MOLECULAR DYNAMICS

Packing strongly influences the electronic properties of materials. Although the details are system specific, it is well-known that organic crystals typically self-assemble into well-defined packing motifs: (1) herringbone, (2) π-stacking, and (3) two-dimensional (2D) brick-like π-stacking.[3,27,28] As tabulated in Table 1 and shown in Figure 2, compounds **1**−**6**, **12**, **14**−**20**, and **22** are packed in a herringbone motif comprising of varying levels of face-to-face and edge-to-face π-stacking. The herringbone packing motif is common in many organic crystals.[3,27,28] Compounds **8** and **13** exhibit a brick-like packing motif with predominant face-to-face stacking, while **7**, **9**, and **10** are packed with a slipped 1D π−π motif. **11** and **21** are comprised of mixed packing arrangements. **11** exhibits a packing arrangement containing slipped face-to-face stacking and face-to-edge (tilted) stacking.[48] The dimers of **21** form a slipped backbone with face-to-edge substituent-backbone π-stacking.[59]

Table 1. Packing Modes for Initial Crystal Configurations of Compounds in Figure 1[a]

compound	acronym	packing mode	ref	$g_{\pi-\pi}$ (%)
1	DNTT	herringbone	12	2.6
2	BB-PTA	herringbone	40	3.3
3	PTA	herringbone	41	3.8
4	DBTDT	herringbone	42	3.1
5	4T/HT	herringbone	43	2.5
6	4T/LT	herringbone	43	2.9
7	DITT	π-stacking	44	2.5
8	PBBTZ	2D π-stacking	45	3.0
9	NTMTI	π-stacking	46	1.8
10	DCV4T	π-stacking	47	2.5
11	TTF	mixed	48	2.9
12	DT-TTF	herringbone	49	3.6
13	HM-TTF	2D π-stacking	50	1.8
14	TTDM-TTF	herringbone	51	3.0
15	DTh-TTF	herringbone	52	2.8
16	NAPH	herringbone	53	3.9
17	ANTH	herringbone	54	3.1
18	TETRA	herringbone	55	3.1
19	PENTA	herringbone	56, 57	2.5
20	PICEN	herringbone	58	2.8
21	DPA	mixed	59	3.5
22	RUBR	herringbone	60	1.5

[a]Paracrystallinity parameter, g (%), calculated for the π-stacking direction of the equilibrated morphologies. 4T/HT and 4T/LT refer to two polymorphs of 4T.

Figure 2 shows representative snapshots from the MD simulations of the morphology of each of compounds **1**−**22**. Only a selected oligomer and its nearest neighbors are shown; everything else is omitted for clarity.

Although there are local structural deformations at the molecular level due to thermal motions, the overall packing motif of each crystal structure is maintained in the MD-equilibrated morphology, in accordance with experimental observations.[12,40−60]

In order to quantify the degree of structural disorder in the equilibrated morphologies caused by thermal fluctuations, we identify the ensemble distributions in centroid distances between dimers of oligomers in the morphologies and identify the paracrystalline order parameter $g = \Delta/d$. Here, δ and d represent the standard deviation and average of intermolecular distance distributions between the backbones of the oligomers, respectively. Paracrystallinity is a measure of cumulative deformation in molecular site positions, and in materials, it is particularly useful for characterizing structural order and defining the crystalline phase.[61,62] It has been recognized that for crystals, $g \sim 0$−1%, for semicrystalline systems, such as polymers, $g \sim$1−8, and for amorphous systems and melts, $g >$ 10%.[61−63]

As shown in Table 1 (see Table S3 for details), for the MD-equilibrated morphologies of the 22 oligomers under study, the g-parameters in the cofacial π-stacking direction ranges from 1.5 to 3.9% with an average value of 2.8%. A g-parameter for TIPS-Pentacene was measured by Rivnay et al.[62] The g = 0.9% value puts TIPS-Pentacene in a crystalline state; this value is smaller than typically estimated for π-stacking direction of compounds **1**−**22**. Based on our simulations, we can infer that the structural order of compounds **1**−**22** fall into a region between far paracrystalline and crystalline state.[63] For the sake of completeness, we also calculated the paracrystallinity g along the face-to-edge packing direction of compounds with the herringbone packing motif and achieved a similar result. Namely, the g parameters range between 1.6 and 3.9% with an average value of 2.8%.

CHARGE-TRANSPORT SIMULATIONS

Transport Mechanism. In this study, we employ the Marcus hopping model to calculate hole mobilities for a diverse set of 22 organic semiconductors. Based on the assumption that charges are localized on a single molecule and charge-transfer reactions take place via an intersite hopping mechanism, the charge-hopping rate is evaluated by the nonadiabatic, high-temperature limit of the Marcus rate for electron transfer:[33,34]

$$k_{ij} = \frac{2\pi}{\hbar} J_{ij}^2 \frac{1}{\sqrt{4\pi\lambda k_b T}} \exp\left[-\frac{(\Delta E_{ij} - \lambda)^2}{4\lambda k_b T}\right] \quad (1)$$

where T is the temperature, $J_{ij} = \langle \phi^i | H | \phi^j \rangle$ is the electronic coupling element (or transfer integral) between the initial $|\phi^i\rangle$ and final $|\phi^j\rangle$ states. λ is the reorganization energy and $\Delta E = \epsilon_i - \epsilon_j$ is the difference in site energies between the initial i and final j states. For efficient charge transport, the electronic coupling element J should be maximized, whereas reorganization energy (λ) and the difference in site energies (ΔE) should be minimized.

The Marcus hopping model has been successfully applied to many systems of organic semiconductors,[23] and is used as part

DOI: 10.1021/ja5076376
J. Am. Chem. Soc. 2015, 137, 2856−2866

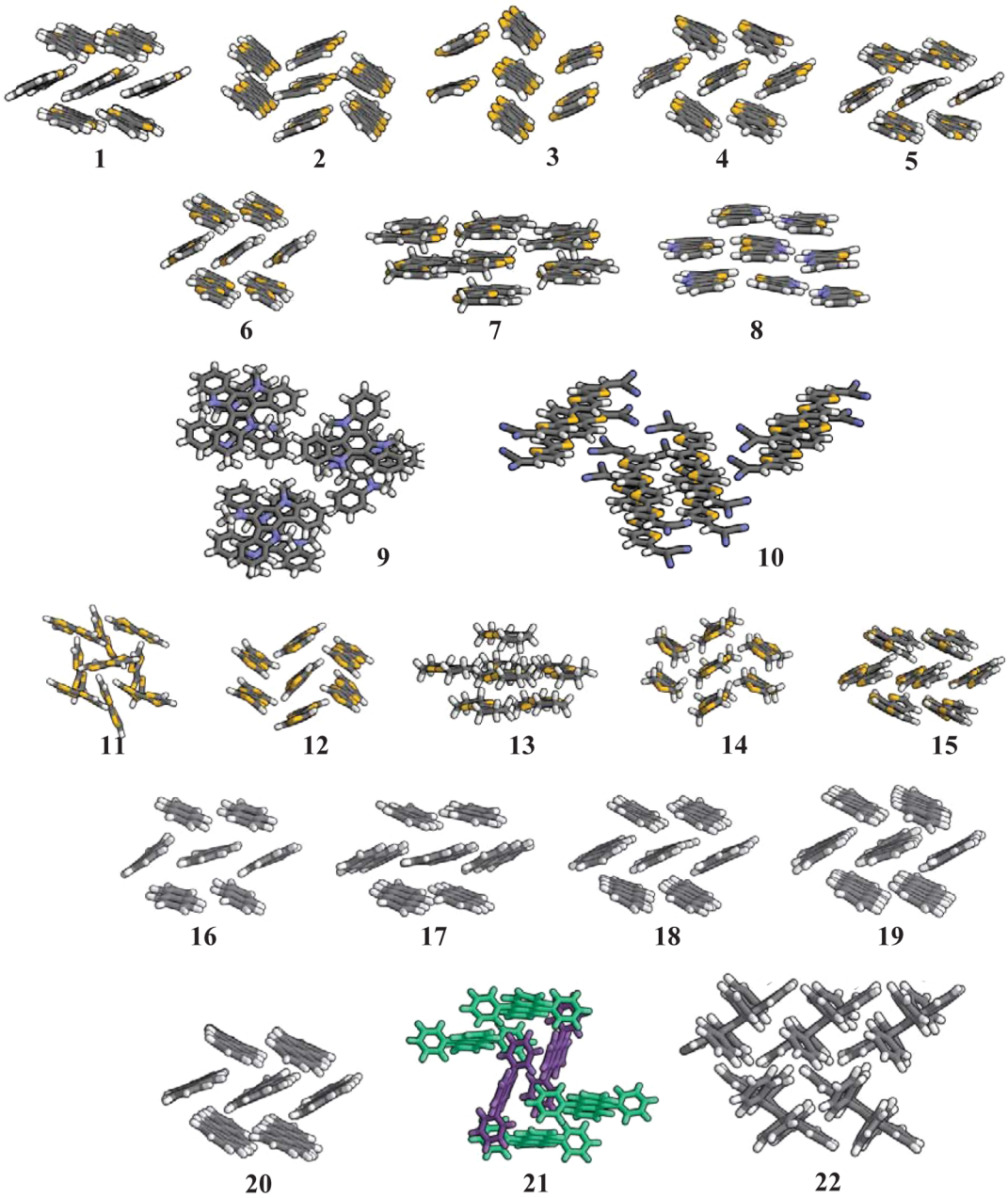

Figure 2. Representative MD snapshots of morphologies **1**−**22**, equilibrated at 300 K. For clarity, only a selected monomer and its nearest neighbors are shown.

of a rational materials design protocol.[30] It has also been applied to elucidate the microscopic charge-transport properties of polymers.[64] Despite the success of charge-transport calculations using the hopping model, the mechanistic origins of charge transport and the theoretical validity of the hopping model to model charge transport in organic crystals are actively debated in the literature.[20,65,66] The major issues with the model are (1) the extent to which localization of the charge-carrier occurs during a charge-transfer reaction in the organic crystal and (2) the appropriateness of the semiclassical treatment that is used by Marcus theory to model charge transport.

The ratio of electronic coupling (J) to reorganization energy (λ), to a rough approximation, is associated with the dominant charge-transport mechanism in a given material. When $J \gg \lambda$, coherent (or delocalized, band-like) transport dominates, but when $J \ll \lambda$, incoherent (or localized, hopping) transport dominates.[24] For most promising materials, however, $J \sim \lambda$, and in these cases, it is unclear whether coherent or incoherent transport is dominant. Due to dynamic disorder resulting from thermal effects at higher temperatures, charge carriers tend to localize and incoherent transport may dominate. Theoretical models[66] and experimental measurements[67] on the scaling of charge mobility to temperature give credence to the appropriateness of using the hopping model to calculate charge mobility around room temperature. In a comparison of localized (Marcus) and delocalized (semiclassical dynamics) models, it was found that simulated hole mobilities do not dramatically differ between the two models, even when one takes into account charge delocalization at room temperature.[23]

The Marcus rate formula deviates from quantum mechanical (QM) behavior at low temperatures, but this deviation is small

DOI: 10.1021/ja5076376
J. Am. Chem. Soc. 2015, 137, 2856−2866

at room temperature. For instance, simulations showed that the charge-transfer rate calculated using the full QM rate formula differ only by a factor of 2−4 at room temperature from the charge-transfer rate calculated using Marcus theory, while the calculated hole mobilities using these two methods differ by a factor of 4−10.[25] The Marcus rate underestimates experimental charge mobility, while the QM rate formula overestimates it (though with less error). Ultimately, neither of the models is accurate within experimental error, and further theoretical and computational efforts are needed to improve the accuracy.

In the following subsections, we will introduce and discuss the key components of Marcus rate calculation: reorganization energy, electronic coupling, and site energies, each of which are evaluated for each dimer of oligomers participating the charge transport. All charge-transport simulations were performed using the VOTCA package.[31,32] A pair of oligomers, for which the intermolecular centroid distances are within a certain interval, are classified as interacting neighbors and added to a *neighbor list* to calculate intersite hopping rates. In this study, we typically use 0.7 nm for the cutoff distance. For some cases, we performed additional simulations with an increased cutoff distance to verify that the results converge.

Reorganization Energies. The reorganization energy (λ) of a molecule undergoing charge transfer has two contributors: inner-sphere (λ_{in}) and outer-sphere (λ_{out}). The inner-sphere reorganization energy (λ_{in}) is the total energy associated with deformation in the nuclear coordinates of the dimer when a charge localized on molecule i is transferred to molecule j. During the charge-transfer reaction in the crystal, the geometry of the surrounding molecules of the dimer may also change, reflected in λ_{out}. For most organic crystals, however, λ_{out} is small and often neglected (i.e., $\lambda \approx \lambda_{in}$). The inner-sphere reorganization energy can be calculated in two ways: (1) from adiabatic potential energy surfaces of isolated monomers or (2) normal-mode analysis. Here we employ the former method throughout the paper. Calculations by Bredás et al. have shown that the two methods yield similar results.[68]

λ is defined by the following expression:

$$\lambda = (E^n_{q_c} - E^n_{q_n}) + (E^c_{q_n} - E^c_{q_c}) \quad (2)$$

where $E^n_{q_n}$ ($E^c_{q_n}$) is the energy of the neutral n (charged c) state of the molecule in its optimized neutral geometry and $E^n_{q_c}$ ($E^c_{q_c}$) is the energy of the neutral n (charged c) state of the molecule in its optimized charged geometry. We perform density functional theory (DFT) calculations, using the B3LYP hybrid density functional[69] with a 6-311G(d,p) basis set as implemented in Gaussian09,[70] to calculate λ for a single isolated molecule.

The DFT-calculated reorganization energies of the oligomers we study here are given in Table 2. The reorganization energies of fused acenes (**16**−**19**) and acene derivatives (**21**, **22**) are rather low and within 100−200 meV, while oligomers without fused benzene rings **3**, **5**, **10**−**15** have rather higher reorganization energies. Reorganization energies of oligomers with heteroaromatic cycles are generally between those of fused and unfused oligomers. The presence of benzene in a heterocyclic oligomer leads to a sizable decrease in its reorganization energy. This is exemplified by comparing compounds **2**−**4**.

Similarly, the presence of the electron acceptor subunits in **10**, dicyanovinyl-substituted (DCV) quaterthiophene (4T), results in a drop in λ of 151 meV compared with quaterthiophene (4T).

Table 2. Reorganization Energies λ, Calculated Using Eq 2 with the B3LYP/6-311G(d,p) Method[a]

	λ	$J_{\pi-\pi}$	J_{tilted}	$\langle J_{\pi-\pi}\rangle$	$\langle J_{tilted}\rangle$	σ
1	134	31	65	32	61	75
2	243	203	0.4	131	0.5	49
3	314	200	0.8	116	0.6	45
4	103	7	31	5	37	77
5	379	4.7	43	4	39	70
6	379	15	21	13	20	88
7	245	21	–	30	–	54
8	197	135	–	320	–	86
9	236	258	–	392	–	71
10	228	73	–	84	–	91
11	288	14	398	41	346	108
12	228	22	40	77	23	53
13	272	61	–	33	–	46
14	274	63	∼0	174	∼0	85
15	399	130	∼0	207	∼0	90
16	189	43	8	36	23	90
17	141	40	26	44	28	82
18	115	29	68	29	66	73
19	95	61	69	32	45	68
20	190	75	71	89	63	82
21	154	396	15	93	50	54
22	160	81	9	75	10	53

[a] $J_{\pi-\pi}$ and J_{tilted} are the modulus transfer integrals for π- and face-to-edge stacking for ideal crystal morphology, $\langle\cdots\rangle$ represents their ensemble averages for equilibrated morphology, respectively. σ is the energetic disorder. All units are in meV.

While **10** and **13** are noticeably planar in the crystal, they are nonplanar in the gas phase.[47,50] Therefore, for **10** and **13**, the reorganization energies were also calculated using constrained geometry optimizations of the ground and charge states. The constraints were necessary as the QM optimizations of those molecules were performed with a single isolated molecule where the absence of neighboring molecules allowed **10** and **13** to relax to ground geometries that show significant twisting along the backbone of the molecules. The constraints were achieved by constraining all torsional angles of **10** and constraining the improper angles of two rigid segments of **13** to the values determined from XRD measurements.[47,50] For **13**, λ from the unconstrained and constrained optimization yield 272 and 239 meV, respectively, whereas for **10** the λ values are 228 and 192 meV, respectively. Because the Marcus rate depends exponentially on λ, a ∼35 meV decrease in λ may lead to a few-fold increase in the Marcus rate.

Electronic Coupling. The transfer integral J in the Marcus rate equation is the electronic coupling between neighboring molecules, which varies with the intermolecular orientations and distances.[14,71,72] Transfer integrals are particularly helpful to quantify the propensity and dimensionality of charge transport in self-assembled systems. Thus, in order to evaluate transfer integrals for a given molecule, knowledge of the atomic-scale material morphology and, consequently, relative positions of neighboring molecules is required. For a perfectly ordered system, it is adequate to calculate electronic coupling J for each unique nearest-neighbor dimer for a given molecule in the unit cell. However, for systems with any disorder, it is necessary to consider huge simulation boxes with a large

DOI: 10.1021/ja5076376
J. Am. Chem. Soc. 2015, 137, 2856−2866

number of molecules to sample all possible configurations. This, in turn, means coping with a large number of dimers with nonzero coupling; on the order of 10^4 or even more. This is computationally prohibitive when one wants to employ first principle methods, since self-consistent field calculations for each pair and individual molecules are required. In this sense, the ZINDO semiempirical method,[70,73] a computationally efficient and robust method, is extremely useful[32,74−77] for computing accurate transfer integrals.

Transfer integrals were calculated between each oligomer and its neighboring oligomers for the unit cell of ideal crystals and for entire equilibrated morphologies. These are given in Table 2 for the face-to-face π−stacking directions and, if present, for the face-to-edge stacking directions. Complete distributions of equilibrated morphologies are provided in Supporting Information. For ideal crystals, the transfer integrals of π−stacking range between 5 and 400 meV. Low J results from weak π−π overlap, usually due to excessive transverse offset or relatively large spacing between dimers. For compounds with herringbone packing, **2**−**3**, **14**−**15**, and **21**−**22**, π−stacking is seen to be the dominant transport direction whereas for **1**, **4**−**6**, **12**, **16**−**20**, and **22**, transfer integrals for both face-to-face and face-to-edge π−stackings are roughly within the same order of magnitude. Although transfer integrals along any transport direction of the equilibrated systems vary due to thermal effects (see Figure S1), when compared with ideal crystal transfer integrals, average values are within the same order of magnitude. For both ideal crystal and equilibrated morphologies, it is interesting to note that the typical electronic couplings for systems with 2D networks are 5−10 times weaker than those of 1D networks. The weaker coupling may seem disadvantageous for these oligomers, but as discussed later, higher-dimensional charge transport with weaker coupling is more advantageous than low-dimensional transport with strong coupling in equilibrated systems.[78]

Site Energies and Energetic Disorder. Site energy is the change in energy of the complex when the charge of the ith molecule changes. The site energy difference ΔE is the change in site energies of molecular pairs i and j participating in the charge-transfer reaction. The site energy difference is zero for perfectly ordered crystals, due to the translational symmetry of each molecule, but it is substantial for partially disordered and amorphous phases. Evaluation of site energies is the most challenging part of calculating Marcus rates because it requires the calculation of multiple subcomponents: the external electric field, Coulombic effects, and polarization effects.[15,32] The straightforward way to evaluate site energy contributors is to consider each atom as point particle with isotropic properties. The evaluation of interaction energies is then carried out in a combinatorial manner.[32] External electric field contributions are calculated using the expression $\Delta E_{ext} = -e\mathbf{F}\cdot\mathbf{d}_{ij}$. Here, $\mathbf{F}$ is the field vector and $\mathbf{d}_{ij}$ is the position vector between molecules i and j. Coulombic and polarization contributions to site energies are calculated using Thole model (for details, see refs 32 and 79−82). Partial charges of neutral and charged states are generated via Merz−Singh−Kollman scheme[83,84] with HF/6-31G(d), based on B3LYP/6-311G(d,p)-optimized geometries, as implemented in Gaussian09.[70] Isotropic atomic polarizibilities of the neutral and charged states are reparameterized for each species to reproduce the molecular polarizibilities obtained from B3LYP/6-311G(d,p).[70] By fitting the histogram of site energy differences to a Gaussian distribution function, the standard deviation, and hence the energetic disorder σ, is evaluated.

The distributions of site energy differences of equilibrated morphologies are depicted in Figure S2, and the energetic disorders extracted from these distributions are given in Table 2. We see from the table that, the energetic disorders for all compounds are nonzero; in fact, they are on the order of ∼50−100 meV, falling into the regime where energetic disorder is typically observed in disordered organic materials (for examples, see refs 18, 85, and 86). The σ = 91 meV calculated for DCV4T (**10**) is in close agreement with Schrader et al.[78] under the same computational platform with different force-field parameters and partial atomic charges. Note that the σ of an oligomer is largely influenced by structural disorder due to fluctuations in intermolecular rearrangements, molecular deformations, and polarization effects. It is difficult to identify which of these effects contributes most to the observed energetic disorder. However, we have identified how the presence of polarization influences the energetic disorder. Although energetic disorder is typically reduced by ∼10% with increased polarization effects, the relatively small σ-values of oligomers **2** and **3** are extreme cases where the polarization effects are substantial. σ is reduced from 78 meV in oligomer **2** and 85 eV in oligomer **3** to 49 and 45 eV with polarization, respectively. Another extreme case is oligomer **16**, where a large σ = 116 meV, which possibly originate from its large paracrystallinity parameter g = 3.9%, reduces to 90 meV with the inclusion of polarization effects. Also, a large σ value for oligomer **11** may arise from its complex topology,[48] although polarization effects reduce σ from 123 to 108 meV. We also observe that energetic disorder linearly decreases with increasing n for oligoacenes **16**−**19**, as the packing motifs of these oligomers are very similar.

MOBILITY CALCULATIONS

Once all of the ingredients of Marcus rates are evaluated and hopping sites are determined, we employ the kinetic Monte Carlo (kMC) method, as implemented in VOTCA,[31,32] to simulate charge-transport dynamics and to evaluate charge-carrier mobility. We calculate the hole mobility for each of oligomers **1**−**22** given in Figure 1, based on three different computational models with increasing levels of disorder introduced into the system. The first model assumes that the experimental material consist of ideal crystals with perfect translational symmetry. Using the second model, we equilibrate the crystal structure at 300 K using MD simulations to introduce structural disorder arising from thermal effects but neglect the energetic disorder from differences in site energies, σ = 0.[15,23,78] The third model incorporates both thermal and energetic disorders into the crystal structure. For each model, we perform kMC simulations to calculate the hole mobility for each oligomer using velocity averaging.[35] For mobility calculations with disordered morphologies, 10 MD snapshots are taken, and for each snapshot we perform 10 separate stochastic kMC simulations. Thus, the hole mobility values calculated using disordered morphologies are averages of 100 kMC runs for each system. To quantify the accuracy of our simulations, we introduce an error function of the form:

$$\Delta = \exp\left[\frac{1}{n}\sum_{i}^{n}\left|\ln\left(\frac{\mu_{\text{theo}}^{i}}{\mu_{\text{exp}}^{i}}\right)\right|\right] \quad (3)$$

DOI: 10.1021/ja5076376
J. Am. Chem. Soc. 2015, 137, 2856−2866

Table 3. Hole Mobilities Calculated for Ideal Crystals and Thermally Equilibrated Morphologies[a]

	computational					experimental			
	our work			others'		crystal		thin-film	
	ideal crystal	equilibrated ($\sigma = 0$)	equilibrated ($\sigma \neq 0$)		ref		ref		ref
1	3.72	2.9	0.91	1.80, 1.90	30, 87	8.3	88	2.9	12
2	7.56	2.59	0.58			0.5	40		
3	3.33	1.14	0.032	0.069	89			0.045	90
4	1.83	0.99	0.1	0.028	89	1.8	42	0.51	91
5	0.19	0.13	0.022	0.021	92	0.23	93	0.014	94
6	0.053	0.060	8.7×10^{-3}	6.2×10^{-3}	92			6.0×10^{-3}	95
7	0.05	0.011	2.3×10^{-3}	0.12	96			1.0×10^{-4}	44
8	1.64	0.78	0.14			3.6	45	0.34	97
9	0.92	0.06	6.6×10^{-3}	0.21	46	0.37	46	8.0×10^{-3}	98
10	1.84	0.3	2.2×10^{-3}	1.1×10^{-3}[b]	78			9.4×10^{-5}	99
11	0.06	0.043	5.0×10^{-4}	0.346	100, 101	0.23	102		
12	1.26	0.52	0.20			1.4	103	0.17	104
13	1.76	0.73	0.208			7.0	50		
14	0.63	0.081	0.011			0.4	51		
15	0.72	0.35	0.033					0.078	52
16	1.59	0.986	0.12	1.32	105	1.0	106		
17	3.46	3.37	0.34	1.84	105	2.93	107	1.1	108
18	2.8	2.3	0.22	4.24, 3.36	105, 109	2.4	110	0.1	111
19	15.6	5.9	0.69	5.37, 4.88, 18.5	105, 109, 35	35	67	3.0	112
20	6.87	8.08	0.64			9.0	113	3.2	114−116
21	8.6	3.7	0.32	2.15	117	3.7	118	0.16	119
22	11.6	7.8	1.94	7.12, 8.1[c], 20	109, 76, 35	15.4	120, 121	1.3	122−124

[a]We compare our predictions with previous computational predictions. [b]Based on the equilibrated morphology with energetic disorder. [c]Equilibrated, without energetic disorder.

The hole mobilities calculated for oligomers **1**−**22**, based on (1) ideal crystals, (2) equilibrated morphologies without, and (3) with energetic disorder, are given in Table 3. Since crystal mobilities are often anisotropic, the table provides the maximum mobility attained among several transport directions. Also, in our simulations we consider "single" charge-carrier dynamics with periodic boundary conditions imposed (i.e., zero charge-carrier concentration). However, experimental hole mobilities are usually observed for high charge-carriers concentrations. Fortunately, this assumption does not lead to a dramatic error for materials with crystalline order.[125]

The hole mobilities of ideal crystal morphologies usually lie in the range of 1−10 $cm^2/(V\ s)$, which is often expected for organic crystals.[3,4] However, we predict a very small ideal crystal hole mobility for **11** ($\mu = 0.06 cm^2/(V\ s)$). This might be attributed to a very complex transport topology with increased vulnerability to charge trapping, even in the ideal crystal. Our ideal crystal mobility predictions usually agree within the same order of magnitude with prior computational studies, except that the mobilities of oligomers 3−6 are roughly 1−2 orders of magnitude higher than the prior studies (see Table 3).

Variations in hole mobilities among oligomers result from the variations in reorganization energies, electronic couplings, and intermolecular spacings. The increases in ideal crystal hole mobilities are accompanied by increases in electronic couplings and intermolecular spacings and decreases in reorganization energies. For example, reorganization energies and electronic couplings along the main transport directions of oligomers **10** (DCV4T) and **20** (Picene) are very similar, but hole mobilities are 1.84 $cm^2/(V\ s)$ and 6.87 $cm^2/(V\ s)$, for **10** and **20**, respectively, since the intermolecular spacing of **20** is greater than that of **10**. The reorganization energies and intermolecular spacings of oligomers **2** (BB-PTA) and **7** (DITT) are also similar, but the hole mobility of **2** is 2 orders of magnitude higher than that of **7**, since modulus square J of **2** is 2 orders of magnitude higher than that of **7**.

Hole mobilities calculated from equilibrated morphologies (but without energetic disorder) are each decreased approximately by a factor of 3. The hole mobility of the equilibrated morphology of oligomer **22** is computed to be 7.8 $cm^2/(V\ s)$, which is in close agreement with the computed value of 8.1 $cm^2/(V\ s)$ by Vehoff et al.[76] We also observe that the magnitude of change in electronic coupling comparing equilibrated morphologies to ideal crystal is not always directly translated into the change in hole mobility, which is clearly an indication of an alternative phenomena. For example, although the J of the ideal crystal and J of the equilibrated morphologies of oligomers **1** and **10** are of the same order of magnitude, the equilibrated hole mobility of **10** is almost an order of magnitude lower than its ideal crystal mobility, while the equilibrated hole mobility of **1** is very close to its ideal crystal mobility. This difference arises from differences in the packing motifs of the two oligomers; even though **10** has a strong π-stacking along the primary transport direction, the electronic coupling of a monomer to its side neighbors is weaker (see Figure S1). The weak horizontal coupling in **10** results in a 1D vertical percolation network through face-to-face $\pi-\pi$ interactions. Vertical (face-to-face) coupling and horizontal (face-to-edge) coupling in crystals of oligomer **1** are almost equal in weight, resulting in 2D transport. In 2D transport, if a hole encounters a trap that makes one of the coupling directions impassable, it may continue traveling in the second direction, while in 1D transport, the hole, upon encountering a trap, will have no such escape route; thus, 2D charge transport is less susceptible to trap states than 1D transport. In summary, we find that hole mobility in oligomers made up of 2D percolation

DOI: 10.1021/ja5076376
J. Am. Chem. Soc. 2015, 137, 2856−2866

networks (see Table 2) is typically a factor of 3 higher than oligomers with 1D networks.

The presence of energetic disorder, arising from the local variations in the geometric structure and electrostatic interactions, creates rougher energetic landscape for charge carriers. A rougher landscape increases the chance of a charge to encounter a transport dead end, which reduces the overall charge-transport efficiency.[126] As Table 3 shows, our results confirm that hole mobility in equilibrated morphologies drops with an order of 10−100 with the inclusion of energetic disorder, caused by an increasing number of trap states. We also find that the influence of the dimensionality of the charge percolation network on hole mobility is even more dramatic for equilibrated morphologies with energetic disorder. That is, the mobility in a high-dimensional network is roughly an order of magnitude higher than mobility in a low-dimensional network. The mobility calculated for oligomer **10** is a factor of 2 higher than found by Schrader et al.,[78] since the energetic disorder we predicted is slightly lower.

Although the influence of reorganization energy λ and energetic disorder σ on hole mobility have both been quantitatively established, our results suggest (see Figure 3) that there is no general relationship between the hole mobility and these parameters in self-assembled systems. Although the trends of regression lines in Figure 3 agree with the general intuition that mobility decreases as λ or σ increase, these parameters poorly correlate with μ. This is expected, as each compound has a unique combination of J, λ, σ, and intersite separation and even the topology.

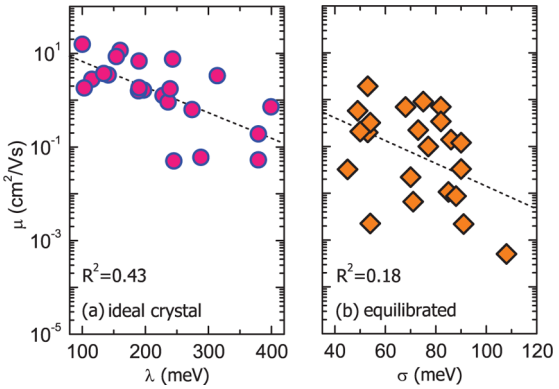

Figure 3. Variation of hole mobility of oligomers with (a) reorganization energy λ and (b) energetic disorder σ. There is almost no correlation between these parameters, suggesting that the packing arrangement plays the crucial role in charge transport.

In the next two subsections, calculated mobilities are compared with available crystal and thin-film mobilities, and interpretations for these findings are given.

Rate-Based Simulations vs Crystal Mobilities. A plot of calculated hole mobility against experimental crystal mobility for each of the 22 oligomers is given in Figure 4a−c. Crystals are materials that exhibit a long-range structural order and their charge-carrier mobilities tend to be higher than their thin-film counterparts, which have shorter range order.[2,27,28] Figure 4a shows the correlation between calculated ideal crystal hole mobilities and experimental crystal mobilities. The hole mobilities span a relatively narrow range of roughly 0.1−10 $cm^2/(V\ s)$, a typical range for crystals with high hole mobilities. The numerical results correlate well with the crystal hole mobility experiments with a Δ = 2.0. As shown in Figure 4b, hole mobilities for equilibrated morphologies, with zero energetic disorder, are calculated to be comparable or slightly lower than those of ideal crystals, resulting in Δ = 2.6 when compared to the experimental crystal data. Finally, our calculations of hole mobility with equilibrated morphologies and energetic disorder compare poorly with experimental crystal values, with Δ = 18.0. Our results suggest that hole mobility in organic crystals with long-range structural order is substantially devoid of the influences from thermal and energetic disorder. That is, the assumption that the crystals exhibit perfect order (due to their highly crystalline order, $g \sim$ 0−1%)[62,63] is not far from including the small structural disorder that is actually present in crystals due to thermal effects.

Rate-Based Simulations vs Thin-film Mobilities. Due to ease of production and relatively good charge-transport characteristics, thin-film materials, with inherent polycrystalline architecture, have been extensively used in organic semiconductor devices. The presence of grain boundaries between crystallite domains is a hindrance to efficient charge transport and is one of the sources of disorder in thin films increasing the likelihood of charge trapping. Although the casting conditions have a strong influence, in most cases mobilities of thin films are lower than mobilities of crystals made from the same materials.[2,27,28]

Figure 5a−c shows the correlation between available thin-film mobility measurements for oligomers **1**−**22** and our calculations based on various morphological assumptions. As shown in Figure 5a, ideal crystal morphologies overestimate thin-film hole mobilities typically by a factor of 19. This is an expected outcome, due to the inherent disorder in thin-film

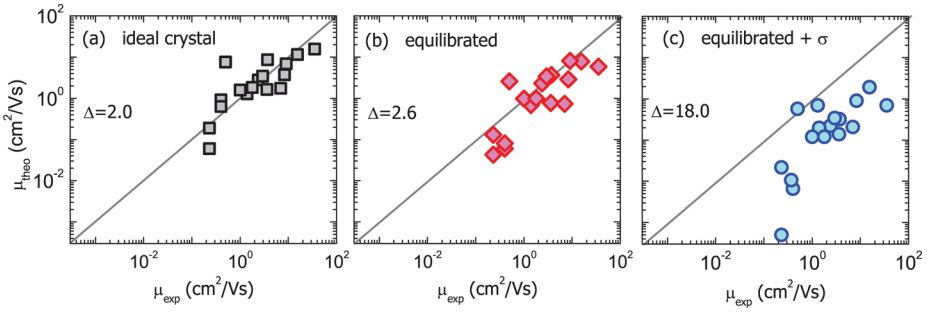

Figure 4. Correlation between experimental crystal and their calculated hole mobilities based on (a) ideal crystal, (b) equilibrated morphology, and (c) equilibrated morphology with site energies. The error function Δ is defined in eq 3.

DOI: 10.1021/ja5076376
J. Am. Chem. Soc. 2015, 137, 2856−2866

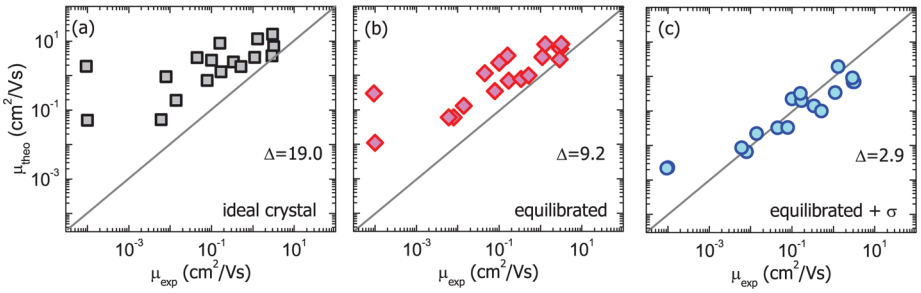

Figure 5. Correlation between experimental thin-film and their calculated hole mobilities based on (a) ideal crystal, (b) equilibrated morphology, and (c) equilibrated morphology with site energies. The error function Δ is defined in eq 3.

morphologies not taken into account by calculations of ideal crystals. The hole mobility predictions are improved by nearly 2-fold when the morphologies are equilibrated at 300 K. Finally, the best reproduction of experimental thin-film hole mobilities, with $\Delta = 2.9$, is obtained from equilibrated morphologies with energetic disorder.

Unlike in crystals with long-range order, the presence of defects in thin films imposes a short-range order. As indicated by our results, in contrast to transport in crystals, disorder-based (σ) transport is essential for charge transport in systems with short-range order.

SUMMARY AND CONCLUSIONS

We have performed charge-transport simulations on a series of π-conjugated systems using three different theoretical models of morphology. These models are ideal crystal, equilibrated morphologies, and equilibrated morphologies with energetic disorder. We found that equilibrated morphologies of these oligomers reside between crystalline and semicrystalline order as identified by experimental crystallographic measurements. The key quantity, hole mobility, has been calculated for each system using these three models. The hole mobility of each system decreases by 1−10-fold with the inclusion of thermal disorder and by a further 10−1000-fold with the inclusion of energetic disorder. We have observed that, among the systems with comparable reorganization energy, the equilibrated morphologies with weak but multidimensional electronic coupling have substantially higher hole mobility than the morphologies with strong but low-dimensional electronic coupling. This effect is attributed to the high probability of dead ends for holes in low-dimensional percolation networks, which are likely bypassed in multidimensional ones. Ideal crystal simulations reproduced the experimental crystal hole mobilities and simulations based on equilibrated morphologies and energetic disorder are in reasonable agreement with experimental thin-film hole mobilities.

Despite the simplicity of the Marcus hopping model, discussions in the literature question the appropriateness of Marcus theory for calculating charge mobility. As a benchmarking study, this work provides more evidence in favor of the hopping model at room temperature. We anticipate that this paper will help inspire further discussion and will contribute to further improvements to models used in the field.

ASSOCIATED CONTENT

Supporting Information

Full names of molecules, initial configurations of MD simulations, direction-resolved paracrystallinity, total electronic energies and optimized geometries of isolated molecules, complete transfer integral, and site energy difference distributions.This material is available free of charge via the Internet at http://pubs.acs.org.

AUTHOR INFORMATION

Corresponding Author

*houk@chem.ucla.edu

Notes

The authors declare no competing financial interest.

ACKNOWLEDGMENTS

The authors are grateful for financial support from National Science Foundation (grant no: DMR-1335645). I.Y. thanks Marmara University and Turkish Higher Education Council (YÖK) for supporting a portion of this research. We thank the developers of VOTCA, especially Denis Andrienko, for helpful discussions and a critical reading of the manuscript. All calculations were performed on the Hoffman2 cluster at UCLA.

REFERENCES

(1) In *Organic Optoelectronics*; Hu, W., Ed.; Wiley-VCH: Weinheim, Germany2013.
(2) Murphy, A. R.; Frechet, J. M. *Chem. Rev.* **2007**, *107*, 1066−1096.
(3) Dong, H.; Wang, C.; Hu, W. *Chem. Commun.* **2010**, *46*, 5211−5222.
(4) Mei, J.; Diao, Y.; Appleton, A. L.; Fang, L.; Bao, Z. *J. Am. Chem. Soc.* **2013**, *135*, 6724−6746.
(5) Kippelen, B.; Brédas, J.-L. *Energy Environ. Sci.* **2009**, *2*, 251−261.
(6) Muccini, M. *Nat. Mater.* **2006**, *5*, 605−613.
(7) Burroughes, J.; Bradley, D.; Brown, A.; Marks, R.; Mackay, K.; Friend, R.; Burns, P.; Holmes, A. *Nature* **1990**, *347*, 539−541.
(8) Müllen, K., Scherf, U. *Organic light emitting devices: synthesis, properties and applications*; Wiley-VCH: Weinheim, Germany, 2006.
(9) Sundar, V. C.; Zaumseil, J.; Podzorov, V.; Menard, E.; Willett, R. L.; Someya, T.; Gershenson, M. E.; Rogers, J. A. *Science* **2004**, *303*, 1644−1646.
(10) Podzorov, V.; Menard, E.; Borissov, A.; Kiryukhin, V.; Rogers, J.; Gershenson, M. *Phys. Rev. Lett.* **2004**, *93*, 086602.
(11) Park, S. K.; Jackson, T. N.; Anthony, J. E.; Mourey, D. A. *Appl. Phys. Lett.* **2007**, *91*, 063514−063514.
(12) Yamamoto, T.; Takimiya, K. *J. Am. Chem. Soc.* **2007**, *129*, 2224−2225.
(13) Yang, H.; Shin, T. J.; Ling, M.-M.; Cho, K.; Ryu, C. Y.; Bao, Z. *J. Am. Chem. Soc.* **2005**, *127*, 11542−11543.
(14) Coropceanu, V.; Cornil, J.; da Silva Filho, D. A.; Olivier, Y.; Silbey, R.; Brédas, J.-L. *Chem. Rev.* **2007**, *107*, 926−952.
(15) Nelson, J.; Kwiatkowski, J. J.; Kirkpatrick, J.; Frost, J. M. *Acc. Chem. Res.* **2009**, *42*, 1768−1778.
(16) Zhao, Y.; Liang, W. *Chem. Soc. Rev.* **2012**, *41*, 1075−1087.
(17) Baumeier, B.; May, F.; Lennartz, C.; Andrienko, D. *J. Mater. Chem.* **2012**, *22*, 10971−10976.

DOI: 10.1021/ja5076376
J. Am. Chem. Soc. 2015, 137, 2856−2866

(18) Hoffmann, S. T.; Jaiser, F.; Hayer, A.; Bässler, H.; Unger, T.; Athanasopoulos, S.; Neher, D.; Köhler, A. *J. Am. Chem. Soc.* **2013**, *135*, 1772−1782.
(19) Troisi, A. *Adv. Polym. Sci.* **2009**, *223*, 259.
(20) Schweicher, G.; Olivier, Y.; Lemaur, V.; Geerts, Y. H. *Isr. J. Chem.* **2014**, *54*, 595−620.
(21) Mas-Torrent, M.; Rovira, C. *Chem. Soc. Rev.* **2008**, *37*, 827−838.
(22) Wu, W.; Liu, Y.; Zhu, D. *Chem. Soc. Rev.* **2010**, *39*, 1489−1502.
(23) Vehoff, T.; Baumeier, B.; Troisi, A.; Andrienko, D. *J. Am. Chem. Soc.* **2010**, *132*, 11702−11708.
(24) Atahan-Evrenk, S.; Aspuru-Guzik, A. *Top. Curr. Chem.* **2014**, *345*, 95−138.
(25) Shuai, Z.; Geng, H.; Xu, W.; Liao, Y.; André, J.-M. *Chem. Soc. Rev.* **2014**, *43*, 2662−2679.
(26) Yavuz, I.; Zhang, L.; Briseno, A. L.; Houk, K. *J. Phys. Chem. C* **2015**, *119*, 158−165.
(27) Wang, C.; Dong, H.; Hu, W.; Liu, Y.; Zhu, D. *Chem. Rev.* **2011**, *112*, 2208−2267.
(28) Jiang, W.; Li, Y.; Wang, Z. *Chem. Soc. Rev.* **2013**, *42*, 6113−6127.
(29) Brusso, J. L.; Hirst, O. D.; Dadvand, A.; Ganesan, S.; Cicoira, F.; Robertson, C. M.; Oakley, R. T.; Rosei, F.; Perepichka, D. F. *Chem. Mater.* **2008**, *20*, 2484−2494.
(30) Sokolov, A. N.; Atahan-Evrenk, S.; Mondal, R.; Akkerman, H. B.; Sánchez-Carrera, R. S.; Granados-Focil, S.; Schrier, J.; Mannsfeld, S. C.; Zoombelt, A. P.; Bao, Z.; Aspuru-Guzik, A. *Nat. Comm* **2011**, *2*, 437.
(31) Ruehle, V.; Junghans, C.; Lukyanov, A.; Kremer, K.; Andrienko, D. *J. Chem. Theory Comput.* **2009**, *5*, 3211−3223.
(32) Ruehle, V.; Lukyanov, A.; May, F.; Schrader, M.; Vehoff, T.; Kirkpatrick, J.; Baumeier, B.; Andrienko, D. *J. Chem. Theory Comput.* **2011**, *7*, 3335−3345.
(33) Marcus, R. A. *J. Chem. Phys.* **1956**, *24*, 966−978.
(34) Marcus, R. A. *Rev. Mod. Phys.* **1993**, *65*, 599−610.
(35) Stehr, V.; Pfister, J.; Fink, R.; Engels, B.; Deibel, C. *Phys. Rev. B* **2011**, *83*, 155208.
(36) Salomon-Ferrer, R.; Götz, A. W.; Poole, D.; le Grand, S.; Walker, R. C. *J. Chem. Theory. Comput.* **2013**, *9*, 3878−3888.
(37) Bayly, C. I.; Cieplak, P.; Cornell, W.; Kollman, P. A. *J. Phys. Chem.* **1993**, *97*, 10269−10280.
(38) Wang, J.; Wolf, R. M.; Caldwell, J. W.; Kollman, P. A.; Case, D. A. *J. Comput. Chem.* **2004**, *25*, 1157−1174.
(39) Allen, M. P., Tildesley, D. J. *Computer Simulation of Liquids*; Oxford University Press: Oxford, U.K., 1989.
(40) Yamada, K.; Okamoto, T.; Kudoh, K.; Wakamiya, A.; Yamaguchi, S.; Takeya, J. *Appl. Phys. Lett.* **2007**, *90*, 072102.
(41) Zhang, X.; Côté, A. P.; Matzger, A. J. *J. Am. Chem. Soc.* **2005**, *127*, 10502−10503.
(42) Li, R.; Jiang, L.; Meng, Q.; Gao, J.; Li, H.; Tang, Q.; He, M.; Hu, W.; Liu, Y.; Zhu, D. *Adv. Mater.* **2009**, *21*, 4492−4495.
(43) Siegrist, T.; Kloc, C.; Laudise, R. A.; Katz, H. E.; Haddon, R. C. *Adv. Mater.* **1998**, *10*, 379−382.
(44) Afonina, I.; Skabara, P. J.; Vilela, F.; Kanibolotsky, A. L.; Forgie, J. C.; Bansal, A. K.; Turnbull, G. A.; Samuel, I. D.; Labram, J. G.; Anthopoulos, T. D.; Coles, S. J.; Hursthouse, M. B. *J. Mater. Chem.* **2010**, *20*, 1112−1116.
(45) Hong, W.; Wei, Z.; Xi, H.; Xu, W.; Hu, W.; Wang, Q.; Zhu, D. *J. Mater. Chem.* **2008**, *18*, 4814−4820.
(46) García-Frutos, E. M.; Gutierrez-Puebla, E.; Monge, M.; Ramírez, R.; Andrés, P. d.; Andrés, A. d.; Ramírez, R.; Gómez-Lor, B. *Org. Electron.* **2009**, *10*, 643−652.
(47) Fitzner, R.; Reinold, E.; Mishra, A.; Mena-Osteritz, E.; Ziehlke, H.; Körner, C.; Leo, K.; Riede, M.; Weil, M.; Tsaryova, O.; Weiss, A.; Uhrich, C.; Pfeiffer, M.; Bäuerle, P. *Adv. Funct. Mater.* **2011**, *21*, 897−910.
(48) Ellern, A.; Bernstein, J.; Becker, J. Y.; Zamir, S.; Shahal, L.; Cohen, S. *Chem. Mater.* **1994**, *6*, 1378−1385.
(49) Rovira, C.; Veciana, J.; Santalo, N.; Tarres, J.; Cirujeda, J.; Molins, E.; Llorca, J.; Espinosa, E. *J. Org. Chem.* **1994**, *59*, 3307−3313.
(50) Takahashi, Y.; Hasegawa, T.; Horiuchi, S.; Kumai, R.; Tokura, Y.; Saito, G. *Chem. Mater.* **2007**, *19*, 6382−6384.
(51) Mas-Torrent, M.; Hadley, P.; Bromley, S. T.; Ribas, X.; Tarrés, J.; Mas, M.; Molins, E.; Veciana, J.; Rovira, C. *J. Am. Chem. Soc.* **2004**, *126*, 8546−8553.
(52) Kakinuma, T.; Kojima, H.; Kawamoto, T.; Mori, T. *J. Mater. Chem. C* **2013**, *1*, 2900−2905.
(53) Alt, H. C.; Kalus, J. *Acta Crystallogr.* **1982**, *1*, 2595−2600.
(54) Brock, C. P.; Dunitz, J. *Acta Crystallogr., Sect. B: Struct. Sci., Cryst. Eng. Mater.* **1990**, *46*, 795−806.
(55) Holmes, D.; Kumaraswamy, S.; Matzger, A. J.; Vollhardt, K. P. C. *Chemistry* **1999**, *5*, 3399−3412.
(56) Schiefer, S.; Huth, M.; Dobrinevski, A.; Nickel, B. *J. Am. Chem. Soc.* **2007**, *129*, 10316−10317.
(57) Yoshida, H.; Inaba, K.; Sato, N. *Appl. Phys. Lett.* **2007**, *90*, 181930.
(58) De, A.; Ghosh, R.; Roychowdhury, S.; Roychowdhury, P. *Acta Crystallogr., Sect. C: Struct. Chem.* **1985**, *41*, 907−909.
(59) Langer, V.; Becker, H.-D. *Z. Kristallogr.* **1992**, *199*, 313−315.
(60) Jurchescu, O. D.; Meetsma, A.; Palstra, T. T. *Acta Crystallogr., Sect. B: Struct. Sci., Cryst. Eng. Mater.* **2006**, *62*, 330−334.
(61) Noriega, R.; Rivnay, J.; Vandewal, K.; Koch, F. P.; Stingelin, N.; Smith, P.; Toney, M. F.; Salleo, A. *Nat. Mater.* **2013**, *12*, 1038−1044.
(62) Rivnay, J.; Noriega, R.; Kline, R. J.; Salleo, A.; Toney, M. F. *Phys. Rev. B* **2011**, *84*, 045203.
(63) Hindeleh, A.; Hosemann, R. *J. Phys. C* **1988**, *21*, 4155.
(64) Poelking, C.; Daoulas, K.; Troisi, A.; Andrienko, D. *Adv. Polym. Sci.* **2014**, *265*, 139−180.
(65) Troisi, A. *Chem. Soc. Rev.* **2011**, *40*, 2347−2358.
(66) Ortmann, F.; Bechstedt, F.; Hannewald, K. *Phys. Status Solidi B* **2011**, *248*, 511−525.
(67) Jurchescu, O. D.; Baas, J.; Palstra, T. *Appl. Phys. Lett.* **2004**, *84*, 3061−3063.
(68) Brédas, J.-L.; Beljonne, D.; Coropceanu, V.; Cornil, J. *Chem. Rev.* **2004**, *104*, 4971−5004.
(69) Becke, A. D. *J. Chem. Phys.* **1993**, *98*, 5648−5652.
(70) Frisch, M. J.; Trucks, G. W.; Schlegel, H. B.; Scuseria, G. E.; Robb, M. A.; Cheeseman, J. R.; Scalmani, G.; Barone, V.; Mennucci, B.; Petersson, G. A.; Nakatsuji, H.; Caricato, M.; Li, X.; Hratchian, H. P.; Izmaylov, A. F.; Bloino, J.; Zheng, G.; Sonnenberg, J. L.; Hada, M.; Ehara, M.; Toyota, K.; Fukuda, R.; Hasegawa, J.; Ishida, M.; Nakajima, T.; Honda, Y.; Kitao, O.; Nakai, H.; Vreven, T.; Montgomery, J. A., Jr.; Peralta, J. E.; Ogliaro, F.; Bearpark, M.; Heyd, J. J.; Brothers, E.; Kudin, K. N.; Staroverov, V. N.; Kobayashi, R.; Normand, J.; Raghavachari, K.; Rendell, A.; Burant, J. C.; Iyengar, S. S.; Tomasi, J.; Cossi, M.; Rega, N.; Millam, M. J.; Klene, M.; Knox, J. E.; Cross, J. B.; Bakken, V.; Adamo, C.; Jaramillo, J.; Gomperts, R.; Stratmann, R. E.; Yazyev, O.; Austin, A. J.; Cammi, R.; Pomelli, C.; Ochterski, J. W.; Martin, R. L.; Morokuma, K.; Zakrzewski, V. G.; Voth, G. A.; Salvador, P.; Dannenberg, J. J.; Dapprich, S.; Daniels, A. D.; Farkas, Ö.; Foresman, J. B.; Ortiz, J. V.; Cioslowski, J.; Fox, D. J. *Gaussian 09*, Revision D.01; Gaussian Inc: Wallingford, CT, 2009.
(71) Brédas, J.-L.; Calbert, J. P.; da Silva Filho, D.; Cornil, J. *Proc. Natl. Acad. Sci. U. S. A.* **2002**, *99*, 5804−5809.
(72) Valeev, E. F.; Coropceanu, V.; da Silva Filho, D. A.; Salman, S.; Brédas, J.-L. *J. Am. Chem. Soc.* **2006**, *128*, 9882−9886.
(73) Ridley, J.; Zerner, M. *Theor. Chim. Acta* **1973**, *32*, 111−134.
(74) Kirkpatrick, J. *Int. J. Quantum Chem.* **2008**, *108*, 51−56.
(75) MacKenzie, R. C.; Frost, J. M.; Nelson, J. *J. Chem. Phys.* **2010**, *132*, 064904.
(76) Vehoff, T.; Baumeier, B.; Troisi, A.; Andrienko, D. *J. Am. Chem. Soc.* **2010**, *132*, 11702−11708.
(77) Poelking, C.; Andrienko, D. *Macromolecules* **2013**, *46*, 8941−8956.
(78) Schrader, M.; Fitzner, R.; Hein, M.; Elschner, C.; Baumeier, B.; Leo, K.; Riede, M.; Bauerle, P.; Andrienko, D. *J. Am. Chem. Soc.* **2012**, *134*, 6052−6056.
(79) Thole, B. T. *Chem. Phys.* **1981**, *59*, 341−350.

DOI: 10.1021/ja5076376
J. Am. Chem. Soc. 2015, 137, 2856−2866

(80) van Duijnen, P. T.; Swart, M. *J. Phys. Chem. A* **1998**, *102*, 2399−2407.
(81) Ponder, J. W.; Wu, C.; Ren, P.; Pande, V. S.; Chodera, J. D.; Schnieders, M. J.; Haque, I.; Mobley, D. L.; Lambrecht, D. S.; DiStasio, R. A., Jr.; Head-Gordon, M.; Clark, G. N. I.; Johnson, M. E.; Head-Gordon, T. *J. Phys. Chem. B* **2010**, *114*, 2549−2564.
(82) Ren, P.; Wu, C.; Ponder, J. W. *J. Chem. Theory Comput.* **2011**, *7*, 3143−3161.
(83) Singh, U. C.; Kollman, P. A. *J. Comput. Chem.* **1984**, *5*, 129−145.
(84) Besler, B. H.; Merz, K. M.; Kollman, P. A. *J. Comput. Chem.* **1990**, *11*, 431−439.
(85) Borsenberger, P. M.; Fitzgerald, J. J. *J. Phys. Chem.* **1993**, *97*, 4815−4819.
(86) Fong, H.; So, S.; Sham, W.; Lo, C.; Wu, Y.; Chen, C. *Chem. Phys.* **2004**, *298*, 119−123.
(87) Sánchez-Carrera, R. S.; Atahan, S.; Schrier, J.; Aspuru-Guzik, A. *J. Phys. Chem. C* **2010**, *114*, 2334−2340.
(88) Haas, S.; Takahashi, Y.; Takimiya, K.; Hasegawa, T. *Appl. Phys. Lett.* **2009**, *95*, 022111.
(89) Zhang, S.-F.; Chen, X.-K.; Fan, J.-X.; Ren, A.-M. *Org. Electron.* **2013**, *14*, 607−620.
(90) Xiao, K.; Liu, Y.; Qi, T.; Zhang, W.; Wang, F.; Gao, J.; Qiu, W.; Ma, Y.; Cui, G.; Chen, S.; Zhan, X.; Yu, G.; Qin, J.; Hu, W.; Zhu, D. *J. Am. Chem. Soc.* **2005**, *127*, 13281−13286.
(91) Gao, J.; Li, R.; Li, L.; Meng, Q.; Jiang, H.; Li, H.; Hu, W. *Adv. Mater.* **2007**, *19*, 3008−3011.
(92) Yang, X.; Wang, L.; Wang, C.; Long, W.; Shuai, Z. *Chem. Mater.* **2008**, *20*, 3205−3211.
(93) Reese, C.; Roberts, M. E.; Parkin, S. R.; Bao, Z. *Adv. Mater.* **2009**, *21*, 3678−3681.
(94) Facchetti, A.; Yoon, M.-H.; Stern, C. L.; Hutchison, G. R.; Ratner, M. A.; Marks, T. J. *J. Am. Chem. Soc.* **2004**, *126*, 13480−13501.
(95) Katz, H.; Torsi, L.; Dodabalapur, A. *Chem. Mater.* **1995**, *7*, 2235−2237.
(96) Geng, Y.; Li, H.; Wu, S.; Duan, Y.; Su, Z.; Liao, Y. *Theor. Chem. Acc.* **2011**, *129*, 247−255.
(97) Hong, W.; Wei, Z.; Xi, H.; Xu, W.; Hu, W.; Wang, Q.; Zhu, D. *J. Mater. Chem.* **2008**, *18*, 4814−4820.
(98) Shelton, S. W.; Chen, T. L.; Barclay, D. E.; Ma, B. *ACS Appl. Mater. Interfaces* **2012**, *4*, 2534−2540.
(99) Fitzner, R.; Elschner, C.; Weil, M.; Uhrich, C.; Körner, C.; Riede, M.; Leo, K.; Pfeiffer, M.; Reinold, E.; Mena-Osteritz, E.; Bäuerle, P. *Adv. Mater.* **2012**, *24*, 675−680.
(100) Li, H.; Zheng, R.; Shi, Q. *Phys. Chem. Chem. Phys.* **2011**, *13*, 5642−5650.
(101) Li, H.; Wang, X.; Li, Z.; Zheng, R.; Zhu, Y. *Sci. China: Chem.* **2012**, *55*, 2176−2185.
(102) Jiang, H.; Yang, X.; Cui, Z.; Liu, Y.; Li, H.; Hu, W.; Liu, Y.; Zhu, D. *Appl. Phys. Lett.* **2007**, *91*, 123505−123505.
(103) Mas-Torrent, M.; Durkut, M.; Hadley, P.; Ribas, X.; Rovira, C. *J. Am. Chem. Soc.* **2004**, *126*, 984−985.
(104) Mas-Torrent, M.; Masirek, S.; Hadley, P.; Crivillers, N.; Oxtoby, N.; Reuter, P.; Veciana, J.; Rovira, C.; Tracz, A. *Org. Electron.* **2008**, *9*, 143−148.
(105) Deng, W.-Q.; Goddard, W. A. *J. Phys. Chem. B* **2004**, *108*, 8614−8621.
(106) Warta, W.; Stehle, R.; Karl, N. *Appl. Phys. A: Mater. Sci. Process.* **1985**, *36*, 163−170.
(107) Karl, N.; Marktanner, J. *Mol. Cryst. Liq. Cryst.* **2001**, *355*, 149−173.
(108) Sannigrahi, J.; Bhadra, D.; Chaudhuri, B. *Phys. Status Solidi A* **2013**, *210*, 546−552.
(109) Wen, S.-H.; Li, A.; Song, J.; Deng, W.-Q.; Han, K.-L.; Goddard, W. A., III *J. Phys. Chem. B* **2009**, *113*, 8813−8819.
(110) Reese, C.; Chung, W.-J.; Ling, M.-m.; Roberts, M.; Bao, Z. *Appl. Phys. Lett.* **2006**, *89*, 202108.
(111) Gundlach, D.; Nichols, J.; Zhou, L.; Jackson, T. *Appl. Phys. Lett.* **2002**, *80*, 2925−2927.
(112) Kelley, T. W.; Boardman, L. D.; Dunbar, T. D.; Muyres, D. V.; Pellerite, M. J.; Smith, T. P. *J. Phys. Chem. B* **2003**, *107*, 5877−5881.
(113) Xin, Q.; Duhm, S.; Bussolotti, F.; Akaike, K.; Kubozono, Y.; Aoki, H.; Kosugi, T.; Kera, S.; Ueno, N. *Phys. Rev. Lett.* **2012**, *108*, 226401.
(114) Kawasaki, N.; Kubozono, Y.; Okamoto, H.; Fujiwara, A.; Yamaji, M. *Appl. Phys. Lett.* **2009**, *94*, 043310−043310.
(115) Kaji, Y.; Kawasaki, N.; Lee, X.; Okamoto, H.; Sugawara, Y.; Oikawa, S.; Ito, A.; Okazaki, H.; Yokoya, T.; Fujiwara, A.; Kubozono, Y. *Appl. Phys. Lett.* **2009**, *95*, 183302−183302.
(116) Kawasaki, N.; Kalb, W. L.; Mathis, T.; Kaji, Y.; Mitsuhashi, R.; Okamoto, H.; Sugawara, Y.; Fujiwara, A.; Kubozono, Y.; Batlogg, B. *Appl. Phys. Lett.* **2010**, *96*, 113305−113305.
(117) Watanabe, S.; Shimodo, Y.; Morihashi, K. *Theor. Chem. Acc.* **2011**, *130*, 807−813.
(118) Tripathi, A. K.; Heinrich, M.; Siegrist, T.; Pflaum, J. *Adv. Mater.* **2007**, *19*, 2097−2101.
(119) Zhang, X.; Yuan, G.; Li, Q.; Wang, B.; Zhang, X.; Zhang, R.; Chang, J. C.; Lee, C.-s.; Lee, S.-t. *Chem. Mater.* **2008**, *20*, 6945−6950.
(120) Sundar, V. C.; Zaumseil, J.; Podzorov, V.; Menard, E.; Willett, R. L.; Someya, T.; Gershenson, M. E.; Rogers, J. A. *Science* **2004**, *303*, 1644−1646.
(121) Podzorov, V.; Menard, E.; Borissov, A.; Kiryukhin, V.; Rogers, J.; Gershenson, M. *Phys. Rev. Lett.* **2004**, *93*, 086602.
(122) Qian, X.; Wang, T.; Yan, D. *Org. Electron.* **2013**, *14*, 1052−1056.
(123) Du, C.; Wang, W.; Li, L.; Fuchs, H.; Chi, L. *Org. Electron.* **2013**, *14*, 2534−2539.
(124) Stingelin-Stutzmann, N.; Smits, E.; Wondergem, H.; Tanase, C.; Blom, P.; Smith, P.; de Leeuw, D. *Nat. Mater.* **2005**, *4*, 601−606.
(125) Pasveer, W.; Cottaar, J.; Tanase, C.; Coehoorn, R.; Bobbert, P.; Blom, P.; de Leeuw, D.; Michels, M. *Phys. Rev. Lett.* **2005**, *94*, 206601.
(126) Borsenberger, P.; Pautmeier, L.; Bässler, H. *J. Chem. Phys.* **1991**, *94*, 5447−5454.

DOI: 10.1021/ja5076376
J. Am. Chem. Soc. 2015, 137, 2856−2866